

# 1 A Fast Method for Detecting Rock Blocks and Calculating Volumes 2 and 3D Surface Areas

3 Ali Polat

4 Provincial Directorate of Disaster and Emergency, 58000, Sivas, Turkey

---

## 5 ARTICLE INFO

6  
7 **Keywords:**  
8 Rock segmentation  
9 U-Net  
10 Convolutional Neural Networks  
11 Rockfall  
12 Volume Calculation  
13 3D Surface Area Calculation

---

## ABSTRACT

14 Rockfall events are a type of natural disaster that causes loss of life and property in the world.  
15 The risk of rockfall can be eliminated by using rockfall prevention methods. To choose the most  
16 suitable method, projecting studies should be carried out. This study aims to automatically detect  
17 rock blocks in a region and calculate their volumes and 3D surface areas. For this purpose, U-Net  
18 segmentation method and Python software language were used. DenseNet121 transfer learning  
19 method based on convolutional neural networks was used for feature extraction. The data set  
20 was created from the orthophoto image obtained by an unmanned aerial vehicle (UAV). Using  
21 the random sampling method, 369 images were selected for training and 191 images for testing.  
22 As a result of the analysis, the mean IOU (Intersection Over Union) was calculated as 85% for  
23 training and 84% for testing. The trained model was applied to the study area and 3111 rock  
24 blocks were detected. This file is saved with coordinates and can be open in any GIS software  
25 and its geometrical properties can be calculated. The volumes and 3D surface areas of the rock  
26 blocks were calculated with Python software as  $275.93 \text{ m}^3$  and  $2615.23 \text{ m}^2$ , respectively. With  
can be used to calculate different types of objects.

---

27

## 28 1. Introduction

29 In many parts of the world, loss of life and property is experienced, and large-scale economic losses occur due to  
30 natural disasters. One of these natural disasters is rockfall events. Rockfalls are a type of slope instability in which  
31 blocks of rock confined to discontinuities move very rapidly from the source region (Varnes, 1978; Hutchinson, 1988;  
32 Cruden and Varnes, 1996). Due to the high velocity during the event, rockfalls can be very dangerous for structures  
33 in their route depending on the block size. Although it is a type of disaster that affects small areas, its consequences  
34 can be very serious. That's why rockfall prevention studies are important. There are also studies on this subject in  
35 the literature (Liu et al., 2021; Keskin and Polat, 2022; Ji et al., 2023; Kainthola et al., 2023; Cao et al., 2024). Some  
36 preliminary studies are needed to develop a prevention method. One of them is the detection of rock blocks and the  
37 calculation of their geometric properties. In this study, rock blocks were segmented, and their volumes and 3D surface  
38 areas were calculated. There are various studies on rock segmentation in the literature.

39 In 2006, Dunlop (Dunlop, 2006) developed a technique for characterization of rocks using albedo, colour, tex-  
40 ture and shape features. In that work rocks in natural scenes are segmented and located with an accurate boundary.  
41 For segmentation purpose top-down and bottom-up knowledge are combined, and geologic rock analysis performed

---

ORCID(s): 0000-0002-9147-3633 (A. Polat)

42 successfully.

43 In the study carried out by Song (Song and Shan, 2006) in this field in 2006, segmentation studies of rocks on  
44 Mars were carried out in order to plan the route and determine the landing areas. Texture-based image segmentation  
45 and edge-flow driven active contour has been developed. Wavelet based local transform, multi-resolution histograms,  
46 and inter-scale decision were combined and used for rock segmentation. As a result of the experiments, reliable rock  
47 segmentation results were obtained by Song.

48 The place of visual navigation in planetary rover autonomy is crucial. Rock segmentation is an important and  
49 challenging task for rover autonomy due to the high computational load and real-time requirement. Kuang et al.  
50 (Kuang et al., 2021) propose a rock segmentation network (NI-U-Net++) to aid in the visual navigation of rovers. The  
51 created model consists of two stages. In the first step, called pre-training, synthetic rock images are created and then  
52 the generated images are used to pre-train the NI-U-Net++ network. The second phase, transfer-training, fine-tunes  
53 the pre-trained NI-U-Net++ network with real-life images.

54 Guo et al. (Guo et al., 2022) proposed an adaptive watershed segmentation method based on distance transformation  
55 for blasted rock piles images. They obtained 95.65% segmentation accuracy for limestone and granite rock blocks with  
56 area over 100 cm<sup>2</sup>.

57 Segmentation of rocks is important in mining as well as in geology. Segmentation is used in this area to deter-  
58 mine the size distribution of rock fragments, to organize and optimize blasting, and to reduce environmental impact.  
59 For this purpose, Malladi et al. (Malladi et al., 2014) proposed a simple superpixel algorithm called Superpixels Us-  
60 ing Morphology (SUM), which uses a watershed transformation approach to generate superpixels; and made a study  
61 comparing some of the current superpixel algorithms on rock images.

62 Recently, various deep learning and machine learning algorithms, including Convolutional Neural Networks (CNN),  
63 have been proposed by researchers working on rock segmentation. Karimpouli and Tahmasebi (Karimpouli and Tah-  
64 masebi, 2019) used convolutional autoencoder networks called SegNet for segmentation of digital rock images. Due to  
65 the limited number of rock images, cross-correlation based simulation was applied to increase the number of images.  
66 20 images taken from Berea sandstone were used as dataset. As a result of the tests, they obtained an accuracy value  
67 of 96

68 Xue et al. (Xue et al., 2021) made rock segmentation study for a different purpose; they proposed the rock seg-  
69 mentation visual system to assist Tunnel Boring Machine (TBM) driving. TBM is an essential equipment for digging  
70 long-range tunnels. They applied different deep learning network for semantic segmentation of rocks.

71 In the above studies, rock segmentation was carried out for different purposes. In this study, rock segmentation  
72 was carried out as a necessary preliminary study in the development of rockfall prevention methods. Rock blocks were  
73 detected precisely in a fast, economical and safe way. In addition, the volumes and 3D surface areas of rock blocks were

74 calculated. The methods and algorithms used in the study can be used in many fields such as engineering applications,  
 75 and geological-geomorphological studies.

76 **1.1. Study area**

77 The study area is in the north of Karasar village, which is approximately 156 km away from Sivas city (Fig. 1).  
 78 This area consists of Middle Miocene aged agglomerate and tuff units (MTA 1/25000) (Fig. 2). This unit was defined  
 79 as Adatepe volcanites according to (Yilmaz and Yilmaz, 2004). The unit consists of black, red-brown, and brown-  
 80 black colored basaltic lava flows and less commonly agglomerate and tuffs. The rock blocks in this unit expose a risk  
 81 of rockfall. Lower Miocene aged sandstone-mudstone-limestone units are observed in the settlement area (Karasar  
 82 village) and vicinity.

83 Karasar village is located on the slopes of a hill. The bedrock on the hill is heavily fractured and cracked. There  
 84 are many rock blocks that have fallen from the upper parts of the slope. The sizes of these blocks vary from  $0.5 m^3$  to  
 85  $15 m^3$ . Rapid temperature changes, heavy snow and precipitation, freeze-thaw, earthquake, and human-induced causes  
 86 increase the risk of rockfall in the region.

87 **2. Methodology**

88 Creating the dataset is a big problem for classification or segmentation processes. In this study, Unmanned Air  
 89 Vehicle (UAV) was used to collect data. An orthophoto image of the region was created from aerial photographs  
 90 obtained by UAV. An area was selected to create train images. Rock blocks within this area were labelled and mask  
 91 images were created. Then segmentation process was completed by Python and necessary libraries, and the results  
 92 were converted to the polygon as a vector file. Moreover, the volumes and 3D surfaces of all the rocks were calculated  
 93 (Fig. 3).

94 **2.1. Data preparation**

95 In this study required data was collected by UAV. DJI phantom 3-Pro was used for image acquisition. First, the  
 96 area to be flown is determined, then the necessary parameters for image acquisition are entered by the Pix4d Capture  
 97 software. These parameters were chosen as follows.

- 98 – Flight altitude (altitude): 100 m.  
 99 – Flight speed (speed): Fast  
 100 – Camera angle (Angle):  $70^\circ$   
 101 – Overlap: 80%

102  
 103 The flight was carried out by the "Double Grid" method. The model of UAV used in this study does not have an

104 obstacle detecting feature. Therefore, when determining the height, it is necessary to pay attention to the nearby power  
105 lines, tall buildings, trees, and peaks of hills.

106 The camera model (FC00X) of UAV has 4000x3000 resolution, 3.61 mm focal length and 1.56 x 1.56  $\mu\text{m}$  pixel  
107 dimensions. After the flight, 284 images were obtained, and these images were processed with the Pix4Dmapper  
108 software. As a result, an orthophoto image with a resolution of 3.51 cm/pixel and a dimension of 2329x1587 was  
109 created.

110 An area was selected to create train and test images from large orthophoto image. This area was selected randomly.  
111 Then all rocks seen on the image were drawn on by GIS software. This file was saved as a vector file and used as mask  
112 data in segmentation processes. After this process, we have created the image and mask files. A deep learning model  
113 requires the same sizes of images. That's why a single image needs to be split into patches. The patch dimension was  
114 used as 256x256. Train-test splitting size was selected as 66% for training data and 34% for testing data. The large  
115 image was split into 9 part to avoid sampling from the same regions. Areas 1,5,9 were selected for creating test images.  
116 Train images were selected from the others (2,3,4,6,7,8) areas (Fig. 4). A total of 600 images (256x256) were selected,  
117 369 images for training and 191 images for testing. The same processes were applied to extract the mask images.

118 We also used the Albumentations (Buslaev et al., 2020) method for data augmentation during the model-building  
119 stage. Albumentations includes many transform methods. We applied augmentation methods given below:

- 120 – horizontal flip
- 121 – affine transforms
- 122 – perspective transforms
- 123 – brightness/contrast/colours manipulations
- 124 – image blurring and sharpening
- 125 – gaussian noise

126

## 127 **2.2. Model building**

128 In this study, U-Net architecture (Ronneberger et al., 2015) was used as a segmentation model. This architecture  
129 is a type of fully convolutional network developed for biomedical image segmentation. It is named U-Net because the  
130 shape of the architecture is like the letter U. The network architecture of U-Net is shown in Figure 5. It consists of two  
131 parts. These are the contracting path (left side) and expanding path (right side). The first part captures context, and the  
132 second part enables precise localization. The left side consists of 4 blocks and each block contains two 3x3 convolution  
133 layers + activation function (with batch normalization) and one 2x2 max-pooling layer. Also, the right side consists of  
134 4 blocks. These blocks include the steps of deconvolution layer, merging with feature map from subsampling path, 3x3

<sup>135</sup> convolution layer + activation function (with batch normalization). Finally, an additional 1x1 convolution operation  
<sup>136</sup> is applied to reduce the feature map to the required number of channels and generate the segmented image.

<sup>137</sup> DenseNet121 transfer learning models were used for feature extraction and rock segmentation was performed with  
<sup>138</sup> U-Net. Segmentation model was evaluated in terms of Intersection over Union (IoU) and F1-score metrics. For the  
<sup>139</sup> calculate loss value dice loss was used. IoU, which is frequently preferred in segmentation problems, is also known as  
<sup>140</sup> the Jaccard similarity coefficient (Jaccard, 1912). It is the ratio of correctly classified pixels to the sum of the number  
<sup>141</sup> of pixels in that class and the predicted number of pixels (Equation 1).

$$J(A, B) = \frac{|A \cap B|}{|A \cup B|} \quad (1)$$

<sup>142</sup> The F1-Score is important in that it is not False Negative or False Positive, but a measurement metric that includes all  
<sup>143</sup> error costs. It is the harmonic mean of Precision and Recall values (Equation 2).

$$F1\text{-}Score = \frac{2 \times \text{Precision} \times \text{Recall}}{\text{Precision} + \text{Recall}} \quad (2)$$

<sup>144</sup>  $\text{Precision} = \frac{TP}{TP + FP}$

<sup>145</sup>  $\text{Recall} = \frac{TP}{TP + FN}$

<sup>146</sup> Where TP is True Positive, FP is False Positive and FN is False Negative.

### <sup>147</sup> 3. Results

<sup>148</sup> In this study, we created our own dataset. A large orthophoto image with a dimension of 2329x1587 was created  
<sup>149</sup> from UAV images. This image needs to be patched for use in the segmentation model. A python script has been  
<sup>150</sup> written for this purpose. It is possible to create the desired number and size of images with the written script. Random  
<sup>151</sup> corner coordinates with the size of 256x256 patches were created. Obtaining images with the exact corner coordinates  
<sup>152</sup> was prevented. Because of this condition, the program gives an error when too many images are wanted to be created.  
<sup>153</sup> Also, the probability of creating very similar images increases. Using the grid method, 56 images can be obtained  
<sup>154</sup> from the large orthophoto image. Using the random sampling method 600 images were obtained from the same image.

<sup>155</sup> U-Net segmentation model was used with DenseNet121. IOU and F1-score values were used as metrics. Model  
<sup>156</sup> parameters were tested with different values. The parameters and values that provide the best results are given in the  
<sup>157</sup> table1 below.

**Table 1**  
Model parameters

Optimizer	Adam
Learning rate	0.0001
Batch size	8
Image size	256x256
Epoch	100

158      IoU scores and losses graph of model is shown in Figure 6. The results of the model are satisfactory for the  
 159      segmentation task. Train IoU, validation IoU, train F1-score and validation F1-score were calculated as 0.8497%,  
 160      0.8461%, 0.9186%, and 0.9152%, respectively.

161      The trained model successfully detected rock blocks in the study area (Fig. 7). The boundaries of 3111 rocks of  
 162      various sizes were determined and created as a vector file (.shp). This method is not recommended for smaller areas.  
 163      Because sufficient training data cannot be created. In areas where there are several rock blocks, detection can also be  
 164      done manually. Sometimes there may be distortions at the edges and corners of the image. This causes errors in rock  
 165      block detection. Therefore, a larger area than the area where the rocks are located should be selected as the study area.

166      After the rocks were detected, each rock's volume and 3D surface area were calculated. These calculations were  
 167      performed using Python. Calculated values were saved in the shape file as fill volume, cut volume and 3D area.

168      In volume calculations, there must be a reference height or surface. In this study, the heights at the boundaries  
 169      of the rocks were selected as the reference height. The calculations were made using an image containing elevation  
 170      data. This image consists of pixels containing elevation values. These pixels form rows and columns. The elevation  
 171      values in each row were used to calculate the total volume. The polygons showing the boundaries of the rocks were  
 172      masked with elevation data. Thus, data with elevation values for each rock were obtained. Volumes were calculated  
 173      by proceeding along the rows. The slope was calculated by comparing the elevation values at the beginning and end  
 174      of the row. A new base elevation was determined for each pixel and the volumes were calculated from this elevation.

175      In this method, it is necessary to evaluate 3 different situations. In the first case, the first height and the last height  
 176      of the rows are equal. The starting elevation value is used as a reference height in this case. The volumes above this  
 177      height are calculated as the fill volume, and the below are calculated as the cut volume. In the second case, the first  
 178      height is greater than the last height of the rows. In the third case, the first height is less than the last height of the  
 179      rows. Different calculations must be made for each situation. These situations are shown in Figure 8.

180      Volume calculation can be easily done by multiplying the pixel area by the height. Heights need to be calculated  
 181      for each pixel. The starting and ending pixels along a row are assumed to be ground. These ground elevations are used  
 182      to find the slope, and each pixel's height is recalculated using this slope. Fill volume and cut volume were calculated  
 183      using new heights and pixel areas. Slopes, fill volumes and cut volumes were determined using the method in Figure

184 X. The total volumes (fill and cut) are found by summing the calculations made for each row.

185 The 3D Surface area was calculated by Python script. Calculations of flat surfaces can be found by multiplying  
 186 pixel lengths. However, different methods must be used for irregular surfaces. The gradient method was used in 3D  
 187 surface calculation. Height changes were calculated in X and Y directions, gradient vectors were obtained in each  
 188 direction. Surface areas were calculated by using these vectors. The slope correction equation is used to determine the  
 189 sloped surfaces (Equation 3).

$$\text{slope correction} = \sqrt{1 + \left(\frac{\partial z}{\partial x}\right)^2 + \left(\frac{\partial z}{\partial y}\right)^2} \quad (3)$$

$$\frac{\partial z}{\partial x} = \text{gradient in X direction}, \quad \frac{\partial z}{\partial y} = \text{gradient in Y direction}$$

190 The 3D surface area is calculated as following:

$$\text{3D surface area} = \text{pixel area} \times \text{slope correction}$$

#### 191 4. Conclusions

192 This study aimed to segment rock blocks and calculate the volume and 3D surface areas of the blocks obtained as  
 193 a result of segmentation. The methods used in the segmentation process provided the determination of the boundaries  
 194 of rock blocks with high accuracy rates. In this way, the geometric properties of the blocks were analysed in detail.

195 U-NET deep learning network and DenseNet121 model were used as segmentation methods. The boundaries of  
 196 rock blocks were determined accurately with the trained model.

197 The volume of each rock block was successfully calculated from the data obtained after segmentation. Similarly,  
 198 the 3D surface areas of the blocks were calculated. High-resolution DEM data were used in volume and surface area  
 199 calculations. Determination of block volumes and 3D surface areas is of critical importance, especially for rockfall  
 200 simulations and engineering analyses. In addition, since the outputs of the study are coordinated vector data, they can  
 201 be easily used in any GIS software. It can be a basis for different studies and analyses.

202 This study has presented a reliable method for segmentation and volume/surface area calculations and has also  
 203 directly contributed to engineering applications in terms of determining the physical properties of rock masses. The  
 204 segmentation section of the study is recommended for terrains containing a lot of rock blocks. It is possible to detect

205 rock blocks in a short time. In addition, this method can be used to automatically detect different types of terrain. Deep  
206 learning models usually require a large amount of data for training. A large amount of data can be generated with the  
207 Random Sampling method proposed in this study. Volume and 3D surface area algorithms can be used not only for  
208 rock blocks but also for any object on the field. These algorithms only require precise DEM data and object boundaries.  
209 For example, these calculations can be made for a single rock block. In these calculations, ground heights and object  
210 heights must be determined clearly. When determining the object boundaries, they should be extended towards the  
211 ground. If the boundaries only represent the object, the ground heights will not be considered, and the results will not  
212 be correct. In some cases, the model can draw the boundaries of the rock blocks narrower. In this case, this problem  
213 can be solved by adding buffers to the rock blocks.

214 As a result, this study provides a basis for volumetric and geometric analyses for rock mechanics, geology and  
215 engineering applications, and can be expanded by testing on different rock types and fields in future studies.

## 216 **5. Acknowledgments**

217 The author wants to thank the Prime Ministry Disaster and Emergency Management Authority for supplying or-  
218 thophoto images and geological map.

219 **Code availability section**

220 Name of the code: rock\_segmentation

221 Contact: ali.polat@afad.gov.tr

222 Program language: Python

223 Software required: Python v3.9

224 Program size: 35.7 KB

225 The source codes are available for downloading at the link: [https://github.com/apolat2018/rock\\_segmentation](https://github.com/apolat2018/rock_segmentation)226 **References**

- 227 Buslaev, A., Iglovikov, V.I., Khvedchenya, E., Parinov, A., Druzhinin, M., Kalinin, A.A., 2020. Albumentations: fast and flexible image augmen-  
228 tations. *Information* 11, 125.
- 229 Cao, Z., Liu, Z., Xu, G., Lin, H., Li, X., Nikitas, N., 2024. Risk assessment and prevention for typical railway bridge pier under rockfall impact, in:  
230 *Structures*, Elsevier. p. 106178.
- 231 Cruden, D.M., Varnes, D.J., 1996. Landslide types and processes. *Transportation Research Board, US National Academy of Sciences, Special*  
232 *Report 247*, 36–75.
- 233 Dunlop, H., 2006. Automatic rock detection and classification in natural scenes. *Masters Thesis, Carnegie Mellon University* .
- 234 Guo, Q., Wang, Y., Yang, S., Xiang, Z., 2022. A method of blasted rock image segmentation based on improved watershed algorithm. *Scientific*  
235 *Reports* 12, 7143.
- 236 Hutchinson, J., 1988. Morphological and geotechnical parameters of landslides in relation to geology and hydrogeology, landslides, in: *Proceedings*  
237 *of the fifth international symposium on landslides*, pp. 3–35.
- 238 Jaccard, P., 1912. The distribution of the flora in the alpine zone. 1. *New phytologist* 11, 37–50.
- 239 Ji, Z.M., Chen, T.L., Wu, F.Q., Li, Z.H., Niu, Q.H., Wang, K.Y., 2023. Assessment and prevention on the potential rockfall hazard of high-steep  
240 rock slope: a case study of zhongyuntai mountain in lianyungang, china. *Natural Hazards* 115, 2117–2139.
- 241 Kainthola, A., Pandey, V.H.R., Singh, P., Singh, T., 2023. Stability assessment of markundi hills using q-slope, smr and simulation tools, in:  
242 *Landslides: Detection, Prediction and Monitoring: Technological Developments*. Springer, pp. 87–107.
- 243 Karimpouli, S., Tahmasebi, P., 2019. Segmentation of digital rock images using deep convolutional autoencoder networks. *Computers & geosciences*  
244 126, 142–150.
- 245 Keskin, İ., Polat, A., 2022. Kinematic analysis and rockfall assessment of rock slope at the unesco world heritage city (safranbolu/turkey). *Iranian*  
246 *Journal of Science and Technology, Transactions of Civil Engineering* 46, 367–384.
- 247 Kuang, B., Wisniewski, M., Rana, Z.A., Zhao, Y., 2021. Rock segmentation in the navigation vision of the planetary rovers. *Mathematics* 9, 3048.
- 248 Liu, W.l., Dong, J.x., Xu, H.h., Sui, S.g., Yang, R.x., Zhou, L.s., 2021. Trajectory analysis and risk evaluation of dangerous rock mass instability of  
249 an overhang slope, southwest of china. *Advances in civil engineering* 2021, 7153535.
- 250 Malladi, S.R.S., Ram, S., Rodríguez, J.J., 2014. Superpixels using morphology for rock image segmentation, in: *2014 Southwest Symposium on*  
251 *Image Analysis and Interpretation*, IEEE. pp. 145–148.
- 252 Ronneberger, O., Fischer, P., Brox, T., 2015. U-net: Convolutional networks for biomedical image segmentation, in: *Medical image computing and*  
253 *computer-assisted intervention–MICCAI 2015: 18th international conference, Munich, Germany, October 5–9, 2015, proceedings, part III* 18,  
254 *Springer*. pp. 234–241.

Short title

- 255 Song, Y., Shan, J., 2006. A framework for automated rock segmentation of the mars exploration rover imagery. URL: <https://api.semanticscholar.org/CorpusID:39798752>.
- 256
- 257 Varnes, D., 1978. Slope movement types and processes. *Landslides: analysis and control* .
- 258 Xue, Z., Chen, L., Liu, Z., Lin, F., Mao, W., 2021. Rock segmentation visual system for assisting driving in tbm construction. *Machine Vision and*
- 259 *Applications* 32, 77.
- 260 Yılmaz, H., Yılmaz, A., 2004. Divriği (sivas) yöresinin jeolojisi ve yapısal evrimi. *Türkiye Jeoloji Bülteni* 47, 13–46.

261 **List of Figures**

262 1	Location map . . . . .	12
263 2	Geological map (1/25000 scale geological map of General Directorate of Mineral Research and Ex-	13
264 plorations) (a), rock blocks (b), settlement and rocks (c) . . . . .		
265 3	Workflow diagram . . . . .	14
266 4	Train and test sampling areas. 1,5,9 test sampling area and 2,3,4,6,7,8 train sampling area . . . . .	15
267 5	U-Net architecture . . . . .	16
268 6	DenseNet121 IoU and Loss values . . . . .	17
269 7	Result map of the model (a) original view, (b,c,d )zoomed views. . . . .	18
270 8	Volume calculation methods. (a) first height is greater than the last height of the rows,(b) b) first height	
271 is less than the last height of the rows . . . . .	19	

Short title

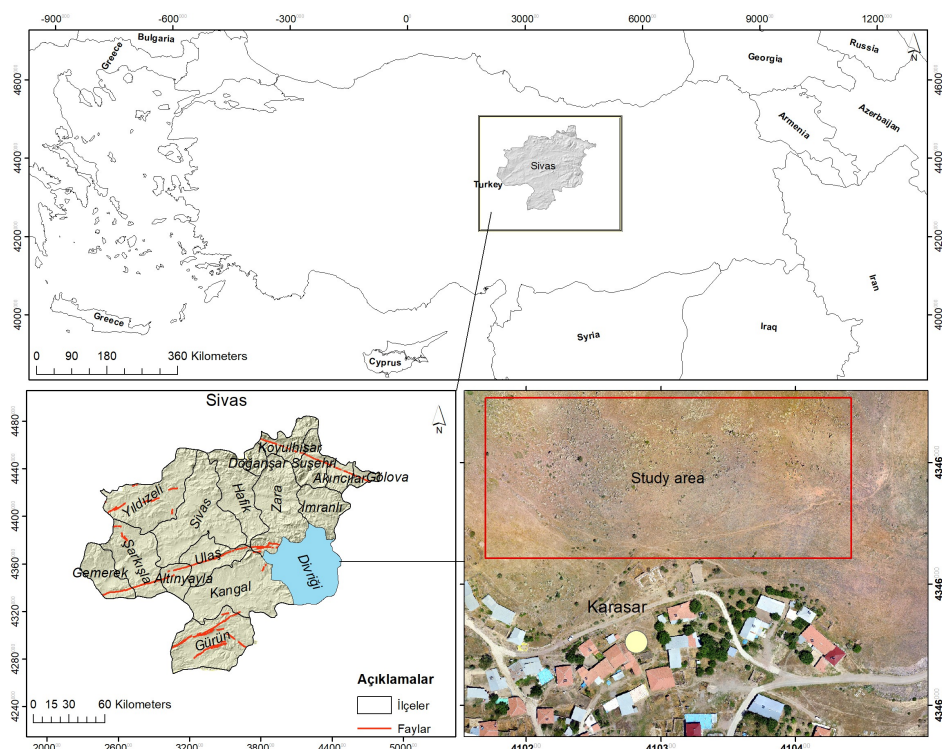
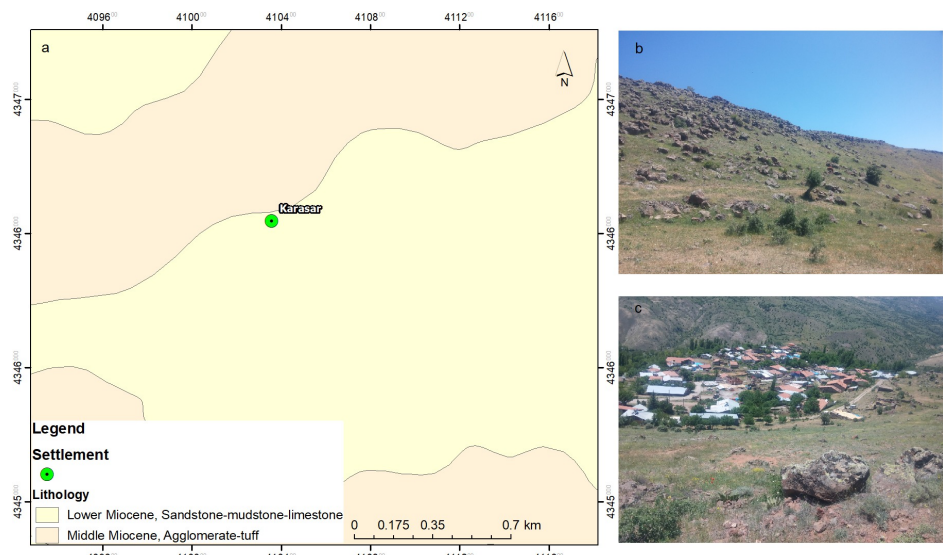
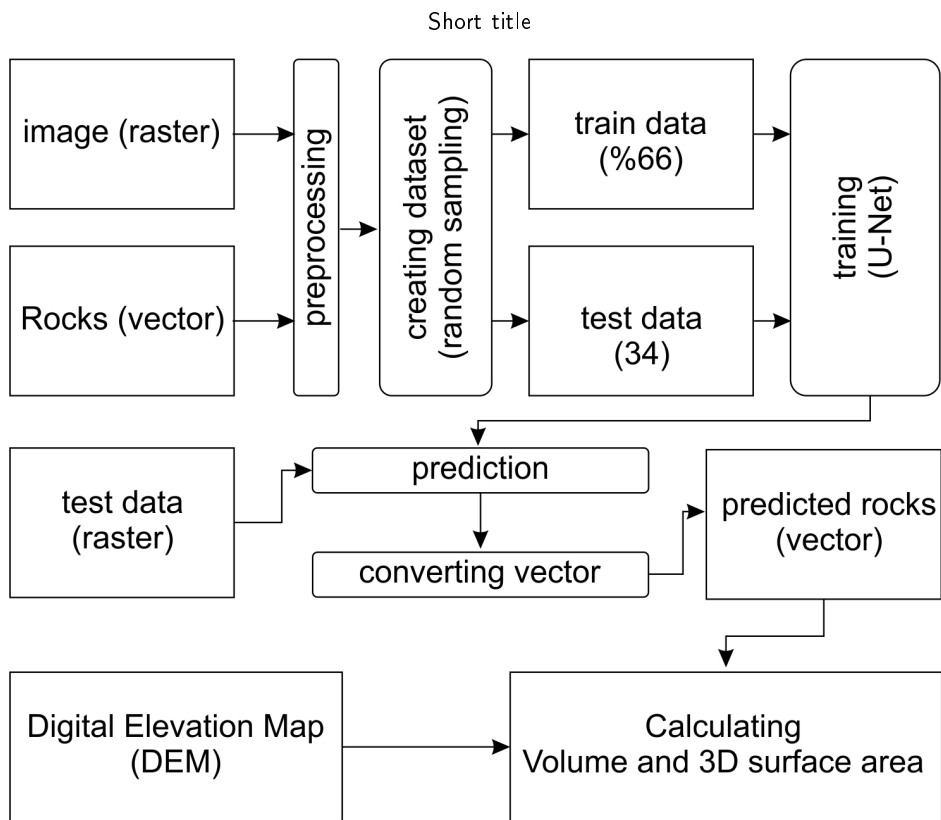


Figure 1: Location map

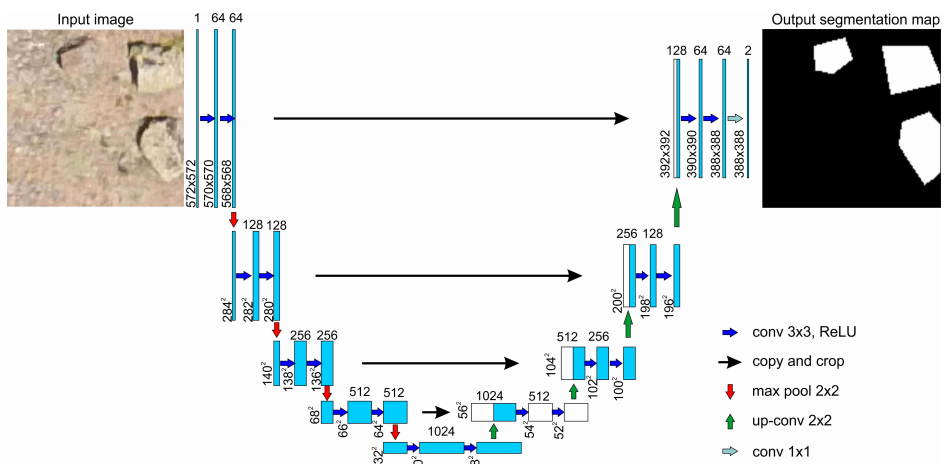




**Figure 3:** Workflow diagram



**Figure 4:** Train and test sampling areas. 1,5,9 test sampling area and 2,3,4,6,7,8 train sampling area

**Figure 5:** U-Net architecture

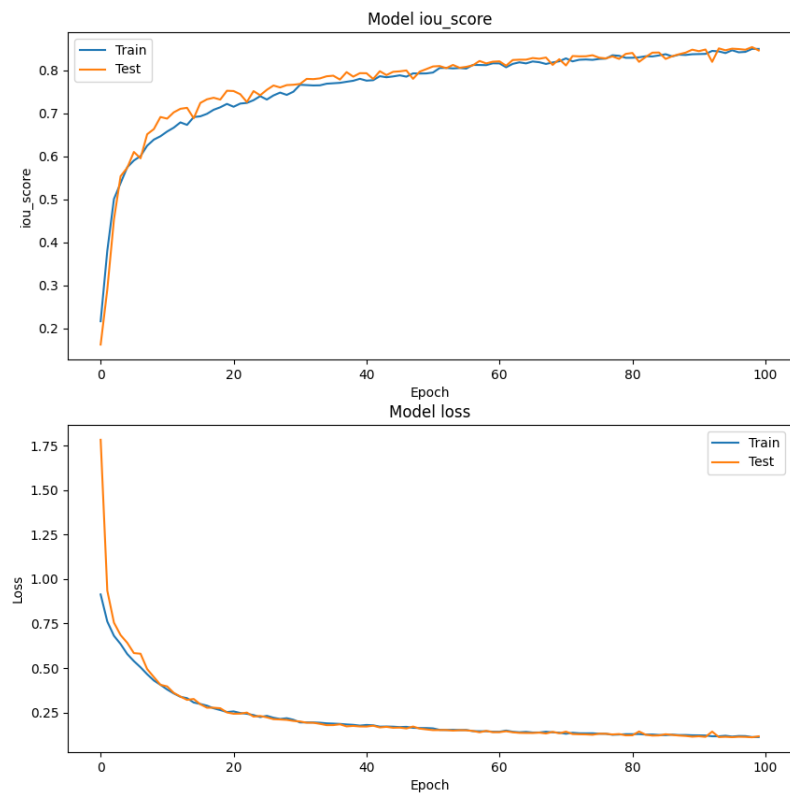


**Figure 6:** DenseNet121 IoU and Loss values

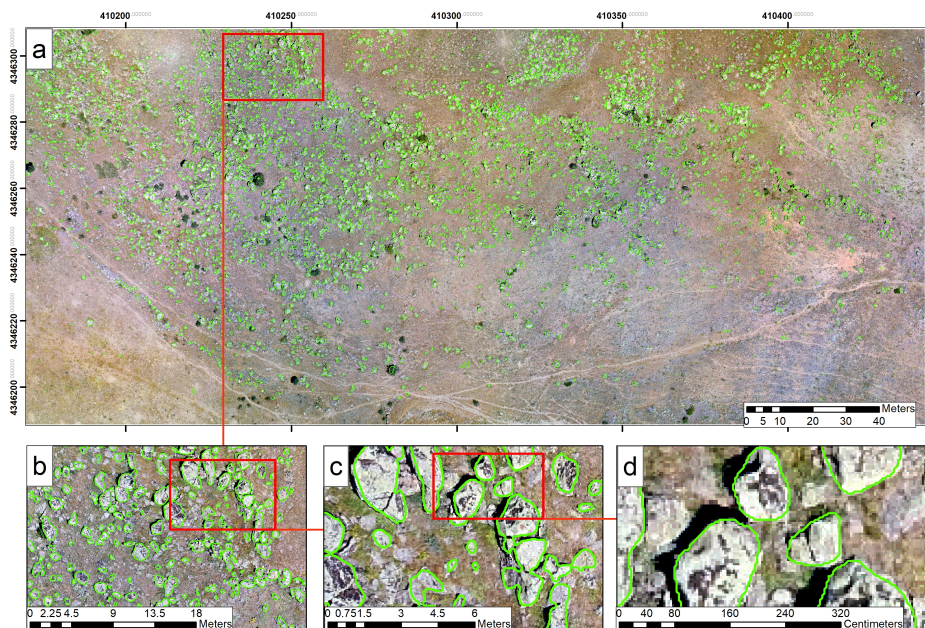


**Figure 7:** Result map of the model (a) original view, (b,c,d )zoomed views.

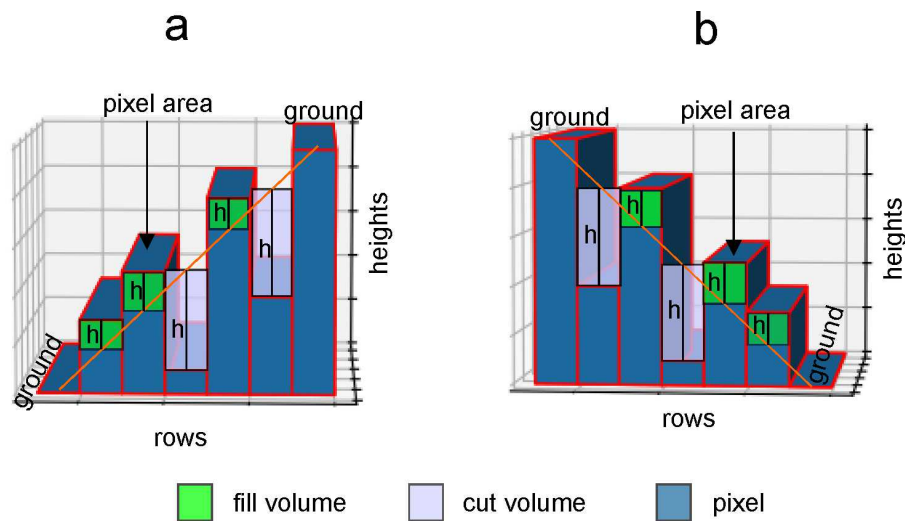


**Figure 8:** Volume calculation methods. (a) first height is greater than the last height of the rows,(b) b) first height is less than the last height of the rows